Journal of Power Sources 188 (2009) 274–280

Contents lists available at ScienceDirect

Journal of Power Sources

journal homepage: www.elsevier.com/locate/jpowsour

Investigation of cell parameters, microstructures and electrochemical behaviour of $LiMn_2O_4$ normal and nano powders

N. Kamarulzaman[a,*], R. Yusoff[a], N. Kamarudin[a], N.H. Shaari[a], N.A. Abdul Aziz[a], M.A. Bustam[b,1], N. Blagojevic[c], M. Elcombe[c], M. Blackford[c], M. Avdeev[c], A.K. Arof[d]

[a] Centre for Nanomaterials Research, Institute of Science, Faculty of Applied Sciences, Universiti Technologi MARA, 40450 Shah Alam, Selangor, Malaysia
[b] Chemical Engineering Programme, Universiti Teknologi Petronas, Bandar Seri Iskandar, 31750 Tronoh, Perak, Malaysia
[c] Australian Nuclear Science and Technology Organization, Lucas Heights Science and Technology Centre, Menai, NSW 2234, Australia
[d] Department of Physics, University of Malaya, 50603 Kuala Lumpur, Malaysia

ARTICLE INFO

Article history:
Received 10 July 2008
Received in revised form 3 October 2008
Accepted 30 October 2008
Available online 27 November 2008

Keywords:
Nano material
Powder diffraction
Neutron diffraction
Sol–gel
Lithium manganese oxide
Lithium-ion battery

ABSTRACT

Nano materials are usually difficult to prepare. This work presents a simple way of preparing $LiMn_2O_4$ nano powders using the high-energy ball milling method. This method has the advantage of producing pure, single-phase and crystalline nano powders. The milling method is carefully controlled to avoid unwanted chemical reactions that may change the stoichiometry of the material. Nano powders of between 30 and 50 nm are obtained. Structural studies of the nano powders, as well as the more conventional micron-sized $LiMn_2O_4$, are made using X-ray diffraction and neutron diffraction methods. Electrochemical evaluation of the materials is undertaken with a three-probe cyclic voltammetry technique and galvanostatic charge–discharge measurements. Structural studies reveal that not only are the crystallites of the nano powders much reduced in size from the normal powders, but their cell parameters are also smaller. The performance characteristics of the nano material show an improvement over that of the micron-sized material by about 17% in the 1st cycle and 70.6% in the 5th cycle, at which the capacity is 132 mAh g^{-1}. The normal material suffers from severe capacity fading but the nano material shows much improved capacity retention.

1. Introduction

The ability to synthesize nano-structured materials has immense implications. To be able to control the building blocks of nature at the atomic and molecular level within the boundaries of the permitted laws of physics is the ultimate ambition of scientists and technologists. This is because designing such materials will enable their functionality to be maximized to unprecedented levels.

Nano materials are expected to exhibit improved functionality [1] due to their high surface area to volume ratio [2]. Particle size seems to be a criterion that affects the electrochemical performance of cathode materials in Li-ion cells [3–5].

It is well known amongst battery material scientists that particle size affects the performance of batteries. For the particle size of normal $LiMn_2O_4$, that is, particle size in the micron range, results from different research groups do not always agree. Yi et al. [6] found that the best-performing material does not come from the smallest group of particles of $LiMn_2O_4$. It was concluded that the material must be carefully optimized. On the other hand, Lu and Lin [7] found that the smaller the particle size, the better is the performance of the battery. For the nano range of $LiMn_2O_4$, the first discharge always shows a higher specific capacity than those from normal materials. Usually, for normal $LiMn_2O_4$ the practical discharge is in the range of 90–120 mAh g^{-1} [6,7], and for nanomaterials about 130–140 mAh g^{-1} [8,9]. The electrochemical behaviour of the nano materials is not that well explained nor understood. For conventional sized particles, the electrochemical properties are believed to be governed by the classical laws of mechanics and electromagnetism. When the particle size is less than 100 nm, however, quantum mechanical aspects may play a part.

The preparation of nano materials usually involves many different processes, the parameters of which have to be optimized. The methods are usually costly, tedious and complex. It is the objective of this work to prepare $LiMn_2O_4$ nano materials using a relatively simple milling method. It is also the aim of the research to make comparisons between the normal and nano powders in terms of their structure and electrochemical performance.

The advantage of the high-energy milling method is that the nano powder is prepared from already pure and single-phase

* Corresponding author. Tel.: +60 3 55444481; fax: +60 3 55443870.
E-mail addresses: norlyk@salam.uitm.edu.my, norlyk3@yahoo.co.uk (N. Kamarulzaman).
[1] Previous address: AMREC, SIRIM Bhd, Kulim, Kedah, Malaysia.

0378-7753/$ – see front matter © 2008 Elsevier B.V. All rights reserved.
doi:10.1016/j.jpowsour.2008.10.139

material. This is different from nano material preparation by a direct synthesis process, especially at low temperatures that normally produce multi-phase products. Therefore, it is expected that the nano materials obtained here will have a high likelihood of being pure, single-phase and stoichiometric as they are obtained from a pure, single-phase and stoichiometric sample.

Several complementary methods of diffraction are used in this study, namely, X-ray diffraction (XRD) and neutron diffraction (ND) techniques. This is to give better ways of comparing the results because the two types of radiation interact differently with matter. As is well known, the scattering factor of X-rays is dependent on the electron density of the atom and thus lithium will not scatter X-rays very much. Therefore, using different diffraction methods, such as neutron diffraction, will give more reliable results and a better understanding of the characteristics of normal (micron-sized) and nano (less than 100 nm) materials. It is also very difficult to elucidate the structure of nano crystalline materials from X-ray powder diffraction (XRPD) as they will give broadened and hence overlapping peaks. Very long scans are needed for good fittings and this is normally impractical. Nowadays, however, laboratory diffractometers fitted with advanced solid-state detectors are capable of taking data about 100 times faster than conventional detectors. Consequently, meaningful XRPD data of the nano powders can be obtained in reasonable times.

Neutron diffraction will give better results for materials containing lighter atoms. This is because neutrons are electrically neutral and can therefore get very close to the nucleus of the atoms, whereas X-rays are more sensitive to the electron cloud of the atom. One disadvantage, however, of using the former method is the difficulty of obtaining neutron beam time.

2. Experimental method

2.1. Preparation of materials

$LiMn_2O_4$ was synthesized by means of the sol–gel method, annealed and stabilized as described elsewhere [10]. The single-phase, crystalline material then served as the starting material to prepare the $LiMn_2O_4$ nano materials.

Preparation of the nano material was via the use of a high-energy planetary ball mill, the Retsch PM 200. The procedure was 10 min of grinding and 5 min of rest. The rest period was to give time for the heat energy to dissipate and ensure that the temperature was kept in check so as to avoid unwanted chemical reactions. It is well known that high-energy ball milling can increase temperatures considerably and cause chemical reactions. The grinding mode was clockwise and anti-clockwise for the production of materials with more homogeneous particle-size distributions. The $LiMn_2O_4$ material was first placed together with balls of 10 mm diameter and tightly closed. Both the holding jars and balls were made of zirconium oxide. The grinding was done using 5.0 g of material with six balls. A milling time of 17 h at a speed of 400 rpm was used.

2.2. Materials characterization—diffraction methods

Structural studies of the materials were undertaken using X-ray and neutron diffraction techniques. The XRD measurements were undertaken with a PanAlytical X'Pert Pro MPD instrument fitted with an advanced solid-state detector called the X'celerator. The bracket and spinner sample holders were used with the Cu K_α radiation and Bragg-Brentano geometry. Neutron data were collected with a Medium Resolution Powder Diffractometer (MRPD) attached to the HIFAR Reactor at the Australian Nuclear Science and Technology Organization (ANSTO). Constant wavelength neutrons were used and the experimental set-up had Debye–Scherer geometry. The Rietveld refinement for the XRD data was performed with PanAlytical software, X'Pert Highscore Plus, while the neutron data was analyzed with GSAS/EXPGUI [11,12].

2.3. Materials characterization—morphological studies

High-resolution transmission electron microscopy (HRTEM) was also performed at ANSTO with a JEOL 2010F (Japan) instrument equipped with a field emission gun (FEG) with an electron source operated at 200 kV. Bright field images and selected area electron diffraction (SAED) patterns were recorded with a 1k × 1k CCD camera in the GIF 2001. The software package Digital Micrograph from Gatan, USA, was used to control the CCD camera. Transmission electron microscope (TEM) specimens were prepared by mixing the powder with acetone and then lightly grinding to form a suspension. A few drops of the liquid were placed on carbon-coated copper TEM grids by means of a pipette, and then allowed to dry.

2.4. Fabrication and electrochemical characterization

Cyclic voltammetry was conducted via the three-probe technique where the $LiMn_2O_4$ was used as the working electrode and lithium metal as the counter and reference electrodes. The electrolyte was $LiPF_6$ in ethylene carbonate (EC)/dimethyl carbonate (DMC) (1:1, v/v: Sol-Rite Mitsubishi Chemical Corp.). The scans were performed at a rate of 0.167 mV s^{-1} (or 10.0 mV min^{-1}) over a range of 3.0–4.5 V using a Solartron 1480 electrochemical measuring equipment.

The electrochemical cell for charge–discharge studies was composed of a composite cathode, a non-aqueous electrolyte, and lithium metal as the anode. The composite cathodes were made up of 76 wt.% of the electroactive $LiMn_2O_4$ mixed with 24 wt.% activated carbon and binder, while the electrolyte was LiPF6 in EC/DMC as stated above. The cathodes were then casted on aluminium grids and compacted using a hydraulic press under a pressure of 81 MPa for 5 min and dried at 393 K for 4 h. The microporous polypropylene separator was soaked in the electrolyte. The composite cathode, electrolyte and Li anode were assembled in a controlled-environment box (M Braun) with an argon atmosphere and water and oxygen contents each of less than 0.1 ppm. Galvanostatic measurements at a current density of 0.3 mA cm^{-2} and over a potential window of 3.0–4.2 V were performed with the same Solartron 1480 electrochemical measuring equipment.

3. Results and discussion

3.1. X-ray and neutron diffraction

The XRPD data were obtained with an appropriate step time and step size in order to obtain acceptable quality data for structural refinement. The measurement specifications used are as shown in Table 1. Nano materials present a problem because long step times are required to get reasonable data. It is, however, quite possible to acquire good measurements with the solid-state detector as this gives reasonable intensities. The peak-broadening effect is still observed due to the decrease in particle size of the nano powders.

The refined XRD patterns of the highly crystalline forms of the normal $LiMn_2O_4$ with bracket and spinner sample holders can be seen in Figs. 1 and 2, respectively. Two sample holder types were used here to check the accuracy and the reliability of the two techniques of data measurements, namely, the normal flat plate (bracket sample holder) and spinning flat plate (spinner sample holder). The former was loaded with the specimens using a front-loading method and the latter with a back-loading method. A Rietveld refinement based on the ICSD 50415 structure showed that the materials were single-phase cubic spinel of the $Fd\bar{3}m$ space group.

Table 1
Measurement and refined parameters for normal and nano $LiMn_2O_4$.

	XRD			ND	ICSD 50415 (ND) Cubic $Fd\bar{3}mZ$
	Normal (bracket)	Normal (spinner)	Nano (spinner)	Normal	
Step size (°)	0.0167	0.017	0.08	0.1	
Step time (s)	30	30	120	360	
a (Å)	8.242(4)	8.245(9)	8.228(4) (−0.2%)	8.243(2)	8.251(4)
Cell volume (Å^3)	559.975	560.675	557.116 (−0.6%)	560.123	561.72
u	0.5091	0.555	0.000	2.439E+2	
v	0.0195	0.000	5.807	1.000E−01	
w	0.0000	0.000	0.000	3.337E+02	
R_B	3.1	4.4	3.1		
R_{wp}	7.4	6.9	7.6	1.8	0.0558
χ^2	2.8	2.7	10.8	2.04	

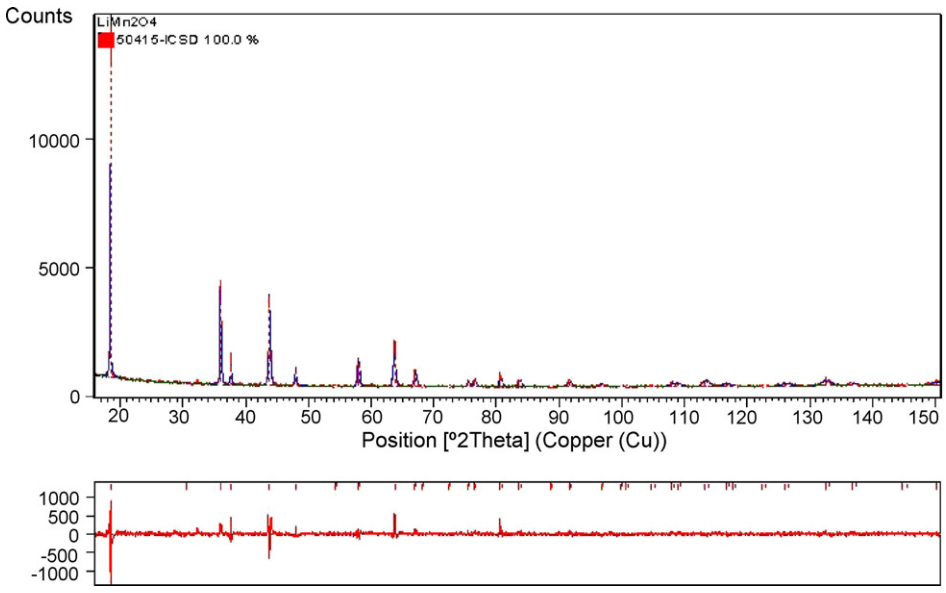

Fig. 1. Refined XRD pattern of normal $LiMn_2O_4$ (bracket).

This agrees well with reported results [13,14] and implies that the cell parameters obtained from the normal crystalline samples have comparable lattice dimensions with $LiMn_2O_4$ obtained via other synthesis routes. The results obtained by the X-ray and neutron techniques for the normal materials are close even though different programming softwares are used (Xpert HighScore Plus and GSAS for X-ray and neutron data, respectively). Fig. 3 shows the refined normal $LiMn_2O_4$ neutron diffraction pattern. The values

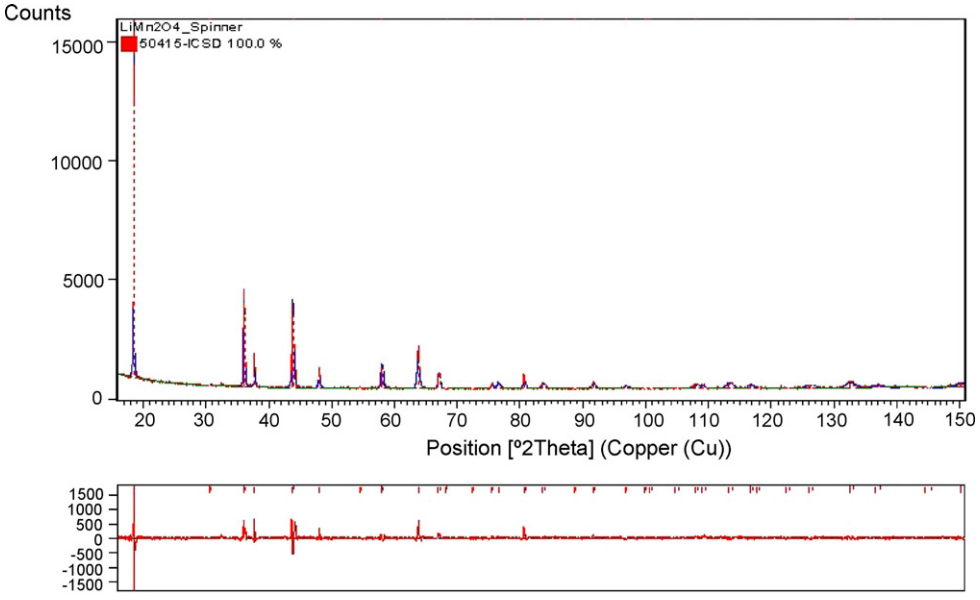

Fig. 2. Refined XRD pattern of $LiMn_2O_4$ (spinner mode).

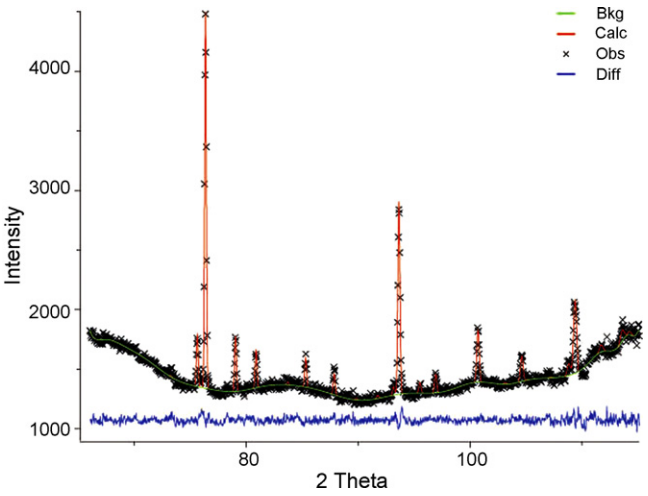

Fig. 3. Refined ND pattern of normal $LiMn_2O_4$.

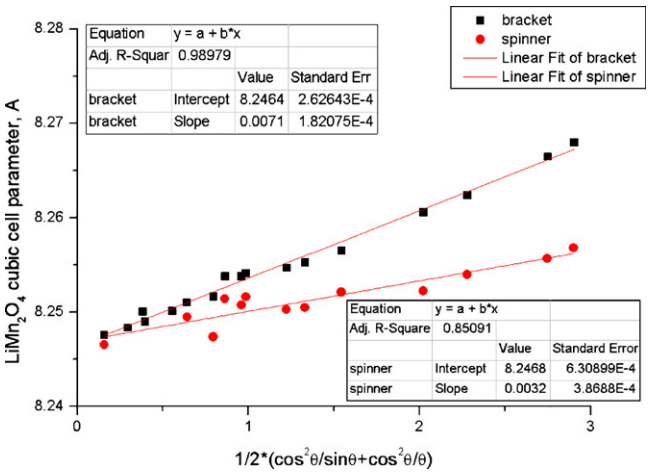

Fig. 5. Nelson–Riley plots of normal $LiMn_2O_4$ (bracket and spinner).

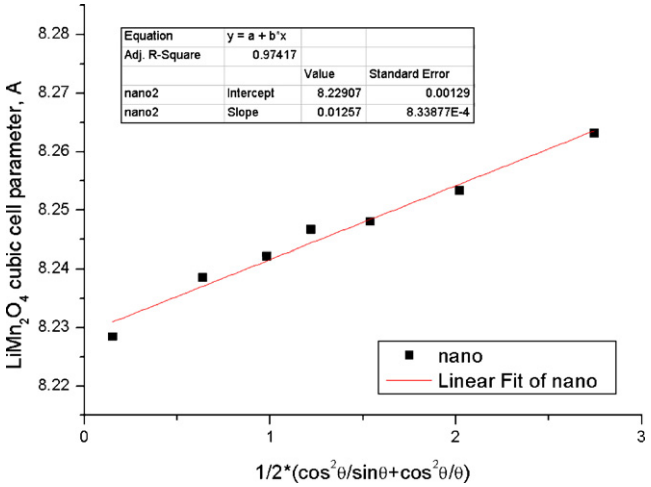

Fig. 6. Nelson–Riley plot of nano $LiMn_2O_4$ (spinner).

of the spinel cubic lattice parameter obtained from XRD data collected in reflection flat-plate and reflection spinning geometries are in excellent agreement with neutron diffraction data. These are represented in Table 1.

The refined XRD pattern of the nano $LiMn_2O_4$ material can be seen in Fig. 4. The cell constant of the nano material is smaller than the normal materials by about 0.2%. This is expected because nano crystals have reduced lattice constants compared with those of normal materials due to the increase in the number of surface ions or atoms to that of the total number of ions or atoms of the crystal [15]. The decrease in the cell volume of the nano material is 0.6% (with reference to the spinner data). A summary of the Rietveld refinement results of the materials is given in Table 1. The Li, Mn and O atoms occupy the usual sites of 8a, 16d and 32e, respectively, with full occupancies. This finding shows that the materials are stoichiometric.

The cell parameters were also evaluated using the Nelson–Riley procedure. This is considered to be a very accurate way of extracting cell constants from XRPD powder patterns, especially for cubic structures [16,17]. Fig. 5 presents plots of the normal $LiMn_2O_4$ obtained from XRD results using the bracket and spinner sample holders, whereas Fig. 6 gives the plot for the nano $LiMn_2O_4$. The values of the cell constants are 8.246 and 8.247 Å for the normal $LiMn_2O_4$ bracket and spinner sample, respectively, and 8.229 Å for the nano $LiMn_2O_4$. The cell parameter for the nano sample is 0.2% smaller than the normal sample (with reference to the spinner

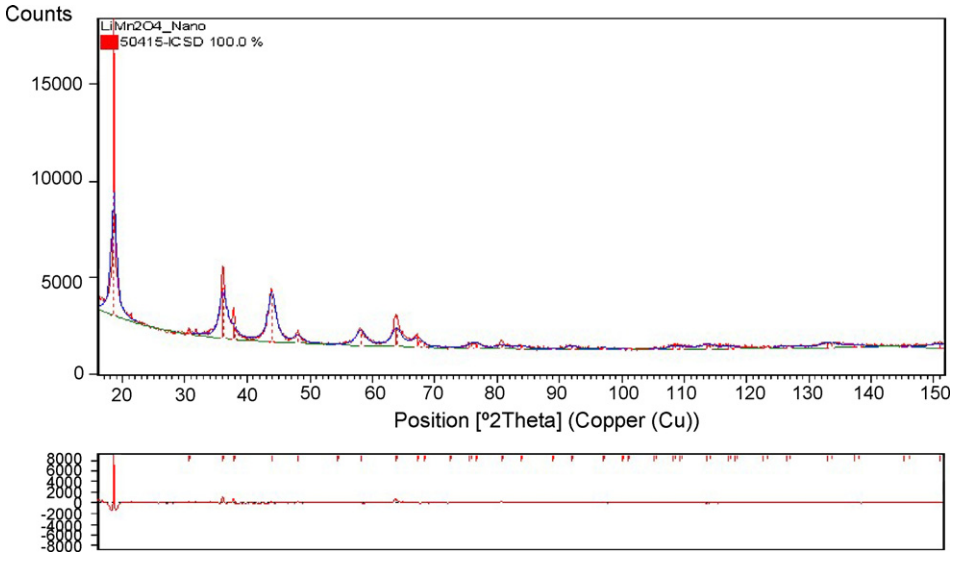

Fig. 4. Refined XRD pattern of nano $LiMn_2O_4$ (Spinner mode).

Table 2
Cell parameters for normal and nano $LiMn_2O_4$ using Nelson–Riley procedure.

	XRD		
	Normal (bracket)	Normal (spinner)	Nano (spinner)
a (Å)	8.246	8.247	8.229 (−0.2%)
Cell volume (Å^3)	560.699	560.903	557.239 (−0.7%)
u	0.5091	0.555	0.000
v	0.0195	0.000	5.807
w	0.0000	0.000	−0.801
R_B	3.1	4.4	3.0
R_{wp}	7.4	6.9	6.1
χ^2	2.8	2.7	6.8

data). The percentage decreases in the cell constant and the cell volume for the nano material as computed by the Nelson–Riley procedure agree with those obtained from the Rietveld refinements of the diffraction data, as can be seen in Tables 1 and 2.

3.2. Morphology

The morphology of the normal $LiMn_2O_4$ crystals can be seen in Fig. 7, which shows a scanning electron micrograph of the material. Some of the crystals have hexagonal, slightly plate-like shapes, while others are more spherical. This indicates that the XRD powder data may contain some preferred orientation effects, especially for measurements taken with the bracket sample holder. The crystallite size is about 0.16–2.0 μm, although the particle size may be larger due to aggregation of the crystallites. Figs. 8 and 9 show transmission electron micrographs of the nano $LiMn_2O_4$. In Fig. 8, the aggregated particles of the nano $LiMn_2O_4$ powders are seen to be composed of tiny crystallites clumped together. A higher resolution micrograph is given in Fig. 9 and reveals that the crystallite size is about 5 nm. This is about ten to a few hundred times smaller than the size of the normal material crystallites. The high-resolution TEM of Fig. 9 proves that the nano materials are crystalline in nature as the lattice spacings can be clearly observed. Thus, this implies that it is possible to obtain diffraction peaks if the counting time is long although the peaks are broadened as can be seen in Fig. 4. Nevertheless, it is believed that the information can be reliably extracted to the limits of the technique.

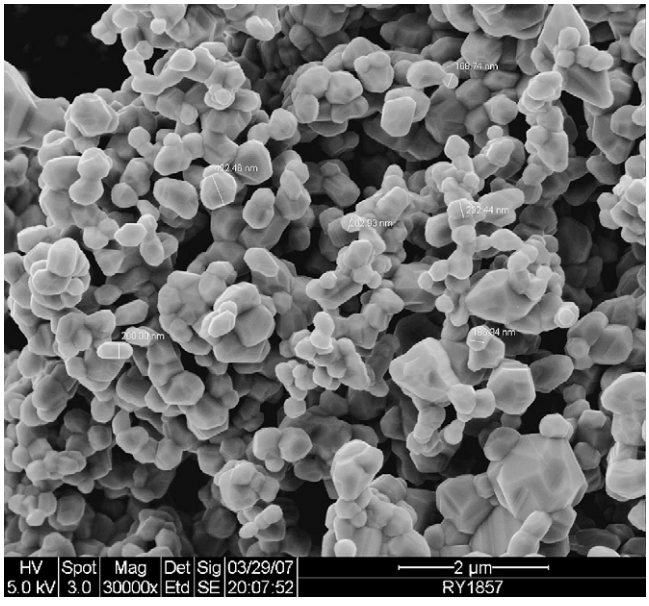

Fig. 7. SEM of normal $LiMn_2O_4$.

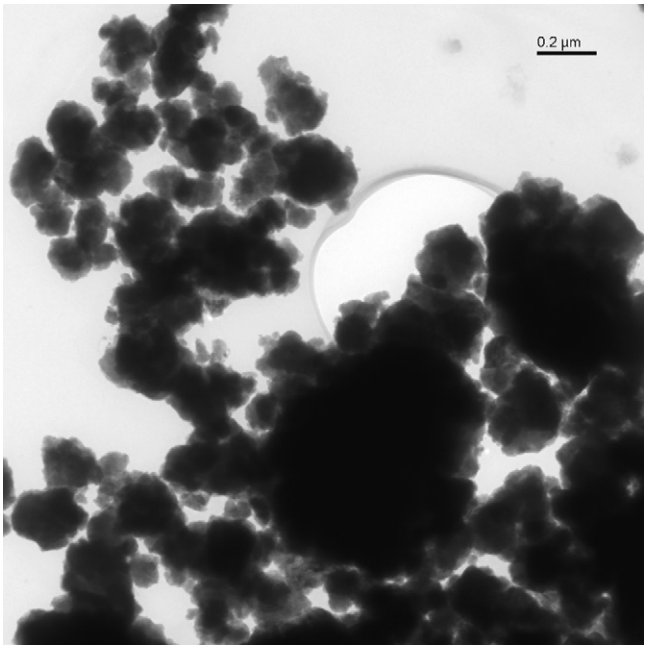

Fig. 8. TEM of nano $LiMn_2O_4$.

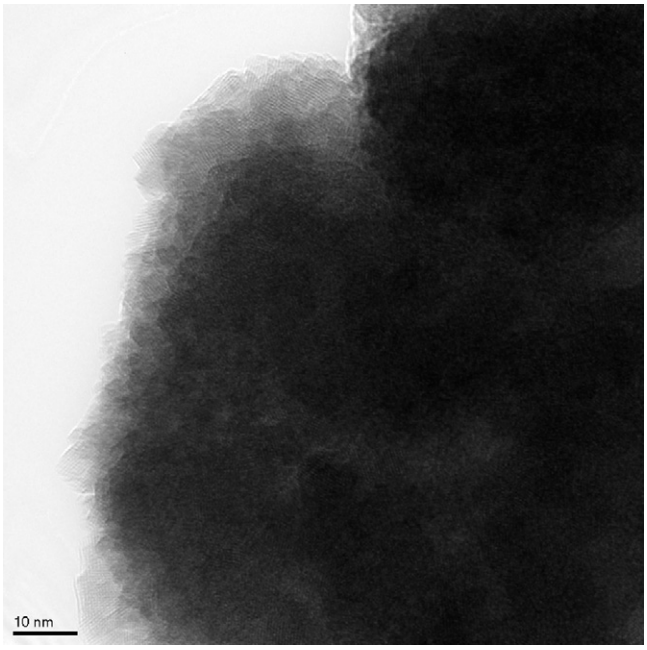

Fig. 9. HRTEM of nano $LiMn_2O_4$.

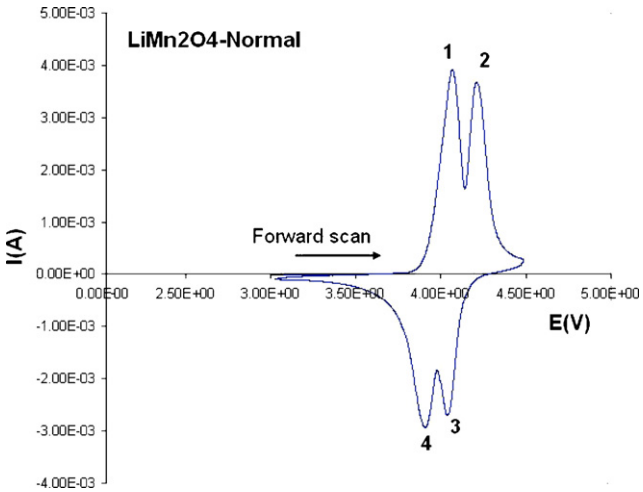

Fig. 10. Cyclic voltmmetry of normal $LiMn_2O_4$.

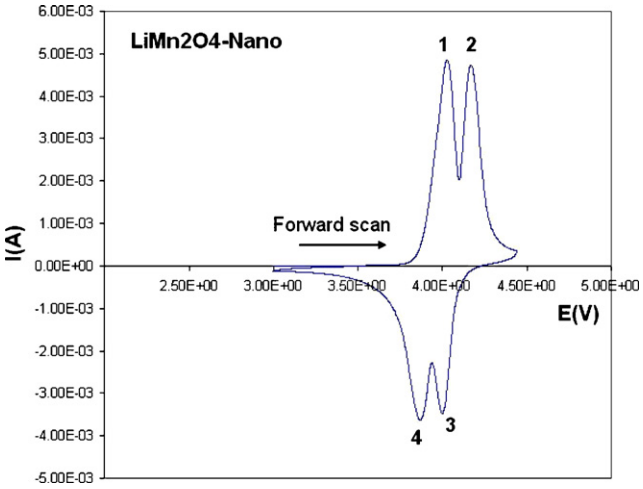

Fig. 11. Cyclic voltmmetry of nano $LiMn_2O_4$.

3.3. Electrochemical characterization

For comparison, cyclic voltammetry has been performed on both the normal and nano materials. The results are given in Figs. 10 and 11, respectively. It is found that the normal and nano $LiMn_2O_4$ exhibit the characteristic double peaks on the forward and backward scans and the peaks are quite sharp. This is indicative of highly crystalline materials [18]. The first peak is attributed to the removal of lithium ions from the tetrahedral sites whereby Li–Li interactions occur, whereas the second peak is attributed to the removal of lithium ions again from the tetrahedral sites but where Li–Li interaction does not occur [18]. The areas under the peaks for the nano materials are approximately equal, but for the normal materials the area of the lower potential peak is higher and indicates that more Li^+ ions are in the tetrahedral sites with Li–Li interaction. This may explain the ease of the de-intercalation/intercalation of Li^+ ions from the crystal lattice. It is also observed that the potential values of the peaks for the nano materials are slightly lower than those for normal materials, that is, by about 1%. The decreases in peak potentials for nano materials agree with reported results of Wu et al. [19] and implies that it takes less energy to extract Li^+ ions from the crystal lattice and to reintroduce it back into the material. The detailed peak potentials for the normal and nano materials and their percentage differences are listed in Table 3. The shift of the peak potentials also accounts for the increase in the specific capacity (as described below) of the nano material.

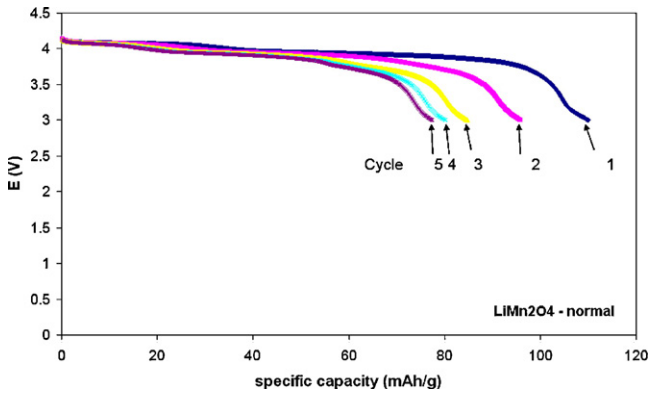

Fig. 12. Discharge of normal $LiMn_2O_4$.

The electrochemical cycleability of the materials was investigated using standard methods of half-cell fabrication and assembling. Charge–discharge was performed over the same voltage range of 4.2–3.0 V. The discharge profiles are shown in Figs. 12 and 13 for the normal and nano materials, respectively. The electrochemical characteristics of the normal material are quite typical of conventional $LiMn_2O_4$ but the discharge behaviour of the nano materials exhibits quite different cycleability over the five cycles. As usual with $LiMn_2O_4$, severe capacity fade occurs from the first to the second cycle, as can be seen in Fig. 12. By contrast, the specific capacity over the same voltage range for the nano materials on the first to the second cycle appears to show an increase of about 3.6%. Thereafter, the capacity fade from the second cycle is only about 0.3% and 0.5% for the fifth cycle. The specific capacities of the materials from the first to the fifth cycle are listed in Table 4. The percentage calculations are done using the first cycle as the reference value. The slight increase in capacity of the second cycle for the nano material is due to the conditioning effects of the cell in the charge–discharge process.

Table 3
Cyclic voltammetric peaks of $LiMn_2O_4$ normal and nano materials.

Sample	$LiMn_2O_4$ normal material		$LiMn_2O_4$ nano material	
	Peak 1 (V)	Peak 2 (V)	Peak 1 (V)	Peak 2 (V)
Forward scan	4.078	4.222	4.037 (−1.0%)	4.180 (−0.9%)
Sample	$LiMn_2O_4$ normal material		$LiMn_2O_4$ nano material	
	Peak 3 (V)	Peak 4 (V)	Peak 3 (V)	Peak 4 (V)
Backward scan	4.030	3.894	3.986 (−1.1%)	3.855 (−1.0%)

Values in brackets are % difference compared with normal materials. Negative sign indicates a decrease.

Table 4
Capacities (mAh g^{-1}) with cycle number and % difference from first cycle discharge.

Sample	Cycle 1	Cycle 2	% difference from 1st cycle	Cycle 3	% difference from 1st cycle	Cycle 4	% difference from 1st cycle	Cycle 5	% difference from 1st cycle
$LiMn_2O_4$ normal	110	95.8	−12.9	84.9	−22.8	80.2	−27.1	77.5	−29.5
$LiMn_2O_4$ nano	129	133.7	+3.6	133.3	+3.3	132.9	+3.0	132.2	+2.5
% difference between nano and normal $LiMn_2O_4$	+17.2	+39.6		+57.0		+65.7		+70.6	

− means decrease, + means increase.

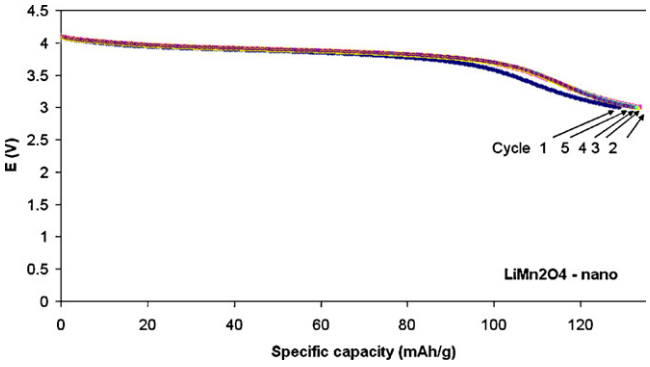

Fig. 13. Discharge of nano $LiMn_2O_4$.

The increase in the specific capacity exhibited by the nano materials can be explained by its small crystallite size, which is very obvious from the HRTEM micrograph. The decrease in size implies an increase in the surface area to volume ratio which, in turn, increases the efficiency of the electrochemical intercalation and de-intercalation of the Li^+ ions in and out of the host material. This is because, when the surface area to volume ratio is larger, the ratio of atoms on the surface to that in the interior is also larger and facilitates the transportation of the Li^+ ions in and out of the crystallite domain. The improved specific capacity can also be attributed to the decrease in cell parameter of the nano materials. This implies a shorter path length that has to be traversed by the Li^+ ions within the crystal domain. This facilitates the transportation of ions through the cathode material into the electrolyte and on to the anode that is required in a lithium rechargeable cell. The small capacity fade over subsequent cycles is also explained by the above reasons, which are believed to have increased the efficiency in the intercalation/de-intercalation process. Intercalation is a phenomenon influenced by this parameter because the dimensions of the crystallite can affect the surface energy of the materials. The surface area to volume ratio is inversely proportional to the linear dimension of the particles and increases by a factor of two in the nano particles. The SEM and TEM results confirmed this. (Assuming a spherical shape, it can be mathematically estimated that the surface area to volume ratio is two orders of magnitude larger for the nano material compared with that of the normal material.) This explains the increased efficiency of the intercalation process in the nano materials, that is, an improved performance of about 17% (in the first cycle) and reduced capacity fade over the five cycles investigated.

4. Conclusion

Nano powders of $LiMn_2O_4$ material prepared by high-energy ball milling are found to be single-phase and stoichiometric with a crystallite size about 100 times smaller than that of the normal $LiMn_2O_4$. This increased the surface area to volume ratio by about two orders of magnitude. Lowering of the surface energy of the nano materials occurs and explains the improved performance and the decrease in capacity fade. The cubic lattice parameters are also smaller for the nano materials that is believed to facilitate the migration of Li^+ ions in and out of the cathode material and results in an increase of cell performance. Another factor that supports the improved performance of the nano materials is the shift of the peak potentials of the nano $LiMn_2O_4$ to lower values by about 1%. The increase in specific capacity in the first cycle is 17%, whereas in the fifth it is 71%.

Acknowledgements

The authors are grateful to the Universiti Technologi MARA and the Australian Nuclear Science and Technology Organization for supporting the sabbatical leave of N. Kamarulzaman, and to the Academy of Science, Malaysia for the research grant; numbered P.20c.

References

[1] J. Schoonman, Solid State Ionics 157 (2003) 319.
[2] S.H. Ju, Y.C. Kang, J. Power Sources 174 (2007) 1161.
[3] P. Barboux, J.M. Tarascon, F.K. Shokoohi, J. Solid State Chem. 94 (1991) 185.
[4] M. Nakayama, K. Watanabe, H. Ikuta, Y. Uchimoto, M. Wakihara, Solid State Ionics 164 (2003) 35.
[5] T. Belin, N. Guigue-Millot, T. Caillot, D. Aymes, J.C. Niepce, J. Solid State Chem. 163 (2002) 459.
[6] T. Yi, D. Wang, K. Gao, X. Hu, Rare Metals 26 (4) (2007) 330.
[7] C.H. Lu, S.W. Lin, J. Power Sources 97–98 (2001) 458.
[8] A. Subramania, Y.C. Kang, J. Power Sources 174 (2007) 1161.
[9] H. Wang, D. Qian, Z. Lu, Y. Li, R. Cheng, Y. Li, J. Phys. Chem. Solids 68 (2007) 1422.
[10] N. Kamarulzaman, Z. Osman, M.R. Muhamad, Z.A. Ibrahim, A.K. Arof, N.S. Mohamed, J. Power Sources 97–98 (2001) 722.
[11] A.C. Larson, R.B. Von Dreele, GSAS, Los Alamos National Laboratory Report Laur 86-748, 2004.
[12] B.H. Toby, J. Appl. Crystallogr. 34 (2001) 210–213.
[13] H. Berg, J.O. Thomas, Solid State Ionics 126 (1999) 227.
[14] P. Piszora, W. Paszkowicz, C. Baehtz, E. Wolska, J. Alloys Compd. 382 (2004) 119–122.
[15] G. Cao, Nanostructures and Nanomaterials, Imperial College Press, London, 2004.
[16] B.D. Gullity, Elements of X-Ray Diffraction, Addison Wesley, Reading, MA, 1978.
[17] H. Lipson, H. Steeple, Interpretation of X-Ray Powder Diffraction Patterns, Macmillan, London, 1968.
[18] W. Liu, G.C. Farington, F. Chaput, B. Dunn, J. Electrochem. Soc. 143 (1996) 879.
[19] H.M. Wu, J.P. Tu, Y.F. Yuan, Y. Li, W.K. Zhang, H. Huang, Physica B 369 (2005) 221.